Journal Name

ARTICLE

Quantitive relationship between fluid inhomogeneities and flow enhancement in nanotubes

Received 00th January 20xx,
Accepted 00th January 20xx

DOI: 10.1039/x0xx00000x

www.rsc.org/

Yuying Wang [a,b †], Junbo Xu [a †], Steven Wang [c], Chao Yang [a,b #]

ABSTRACT: Flow enhancement in nanotubes is of great potential to achieve ultra-fast fluidic transport. But the mechanism of such fast transport and its reduction as the tube enlarges to bulk scale is still unclear. In this work we establish a model to quantitatively correlate the flow enhancement and the fluid inhomogeneity to describe the enhanced transport and its evolution with the tube dimension. We found the fluid inhomogeneity at solid-liquid interface in nanotubes and its independence with tube size by dissipative particle dynamics (DPD) simulation. Based on that, we establish novel theoretical models for the penetration rate in nanotubes with parameters related to the fluid inhomogeneity for the first time, which can achieve quantitatively prediction for nanoflow enhancement and are valid through all scales.

1 Introduction

Flow under nano-confinement is ubiquitous in many fields and its related domains like membrane and catalysis are considered promising to alleviate energy, environmental and resources problems. It is found to be of great potential in fast[1] and selective transport[2] as separation and fluidic diode[3] and expected to break the tradeoff between selectivity and penetration rate for traditional membranes. For instance, Fornasiero *et al.*[4] fabricated a carbon nanotube membrane with a high selectivity at 98%, whose penetration rate reached 1000 times of the Hagen-Poiseuille prediction. Corry *et al.*[5] simulated the membranes incorporating carbon nanotubes which obtained 95% desalination with a flow rate of over 1500 times that of existing membranes.

Numerous works have tried to explain the flow enhancement within nanotubes from many aspects. One explanation is that the carbon nanotubes, which is used in most situations, have surfaces with atomic smoothness[6], leading to surface slippage[7]. In this case, no model can act as the bridge from phenomena to theory. Recently, the negative relation between the slip length and the nanotube radius has been elucidated by Bocquet *et al.*[8]. Which challenges the custom in existing models where the slip length is used as constants[9]. Besides, their results is based on experiments leaving a potential room for theoretical investigation. On the other hand, fluid inhomogeneity are believed to be responsible for the enhancement. Such inhomogeneity can result in the change of friction and lead to superlubricity[10]. Inhomogeneous local viscosity can reflect the friction from another perspective, and it is on one hand calculated from the shear stress and the non-smooth velocity profiles [11,12] and on the other hand measured by the local random walk waiting time[13]. Some models like the two phase model[14] and its modifications[15, 16] have attempted to fix the deviation between the Hagen-Poiseuille relation and the real penetration rate. These models separate the boundary region and assign it with a lower viscosity. Although they can partly explain the enhancement, the setting of the regional viscosity is more empirical than theoretical. In addition, the phonon influence[17] and entropy analysis[18] were also used to elucidate the flow enhancement in nanochannels. But the former is too weak to be the critical reason at about tenfold enhancement with natural oscillation and the latter is only applicable in extremely confined systems, usually smaller than 2 nm in diameter, while the enhancement has been reported in a wider range[19].

With overall consideration, we focus on the fluid inhomogeneity, including the viscosity and density oscillation, and prove it to be the crucial factor that leads to the flow enhancement. In addition, the inhomogeneity also gives rise to apparent slip, which may act as the visualized reason for the flow enhancement.

The Molecular Dynamics (MD) is widely employed in nanofluidic study, but it is not the best choice in this work for a couple of reasons. First, the lack of force field adapted to nanofluidic anomalous arrangement is fatal for the accuracy. Second, the mismatching in length and time units results in the over-fast velocities compared with experimental results. At last, as a rare region with fractional fluid molecules takes place aside the solid interface, the computational steps acquired for a full statistics to depict smooth velocity profiles are enormous. In this work, we use the Dissipative Particle Dynamics (DPD) as the molecular level description of simple liquids, which can efficiently provide reliable results on the level we concern about like fluidic transport and distribution, to assist our theoretical investigation in this work. The scaling of the DPD units to real ones are also performed in the end of the article.

[a] *Key Laboratory of Green Process and Engineering, Institute of Process Engineering, Chinese Academy of Sciences, Beijing 100190, China*
[b] *University of Chinese Academy of Sciences, Beijing 100049, China*
[c] *School of Chemical Engineering and Advanced Materials, Newcastle University, NE1 7RU, UK*
† Yuying Wang and Junbo Xu contributed equally to this work
# Chao Yang: E-mail: chaoyang@ipe.ac.cn; Tel: +86-10-62554558; Fax: +86-10-82544928.
Electronic Supplementary Information (ESI) available: [details of any supplementary information available should be included here]. See DOI: 10.1039/x0xx00000x

Based on the simulation findings, the hydrodynamic equations are re-derived. The theoretical models for both the penetration rate and the apparent slip in nanotubes are established for the first time. The models are verified by the simulation results and applied to the former experimental data.

2 Simulation

In the DPD simulation, we use the parameter a in the inter-particle repulsive forces to denote different kinds of particles. The repulsive parameter between the solid walls and the fluid, a_{sf}, can be used to alter the solid wettability in this work. A series of simulations are conducted to show the positive correlation of a_{sf} and the contact angle (see Fig. S2). Another variable we focus on is the tube radius R. The size of the fluid beads can be charactered by σ_D, the effective diameter of the liquid beads, which is obtained by the radial distribution function as 0.86. The solid walls in this work are constructed by beads in face-centered cubic, which vibrates around each points. The inner two layers are tunable in repulsive parameters to embody different wettabilities. While the outermost layer is assigned with super strong repulsive parameter with the fluidic beads (a_{sf}=50), which can ensure the walls to be impenetrable. Meanwhile, such strong repulsion will have no impact on the fluid within the walls for its distance from the inner surface is a little larger than the cut-off distance. The details about the DPD method and the establishment of the simulation system are presented in the supporting information (SI, sections 1 and 2).

Affected by the solid-liquid interaction, the density profiles are highly non-uniform in the vicinity of the walls. One conclusion we draw from simulation is that such inhomogeneity is independent of the tube radius but depends heavily on the wall wettability. In **Fig. 1a**, the density profiles in the tubes with various radiuses but identical wettability are virtually coincident with each other. Only when the radius is extremely small (R<3σ_D) with the overlapped solid effect do the profiles deviate from the others. In **Fig. 1b**, the intensified inhomogeneity with an inward peak position and a higher peak value can be observed with greater a_{sf} (stronger hydrophobicity). In addition, the driving force is also tested as an effective factor for the density distribution and it turns out to have no impact on it in the velocity range involved in this work (SI, section 3). Therefore, once the solid walls are settled, the density inhomogeneity that starts from the solid-liquid interface is fixed. We define the region aside the walls, involving the apparent waves of density, as the inhomogeneous region. Its thickness δ extends to about 3σ_D in all the cases. The other region with uniform density is known as the bulk region.

Analogous to the density profiles, the velocity profiles are also affected by the solid-fluid interaction. Which is similar to the cases within nanoslits of our previous works[20]. In the bulk region the velocity profile is always in a parabolic pattern which is well established by the Hagen-Poiseuille relation. Nevertheless it gets into distortions in the inhomogeneous region, which enhances the overall velocity to a great level (SI, section 3). The reason why the velocity pattern distorts lies in the viscosity inhomogeneity that is similar to that of density. In a fluid with a single component, a positive correlation is considered to exist between the local viscosity and density, and the viscosity is exclusively related to the density in constant temperature[14]. As a consequence, the viscosity is also independent of the channel size. With the simulated stress based on the Irving-Kirkwood method [11, 21] and the velocity distribution, the local viscosities are calculated and the profiles are shown in **Fig. 1b**. To clarify the accuracy of the density and viscosity results, the normalized density and viscosity profiles of non-equilibrium molecular dynamics[11] are also displayed in Fig. 1b as the dashed lines. Quantitatively resemblance can be found with the profiles.

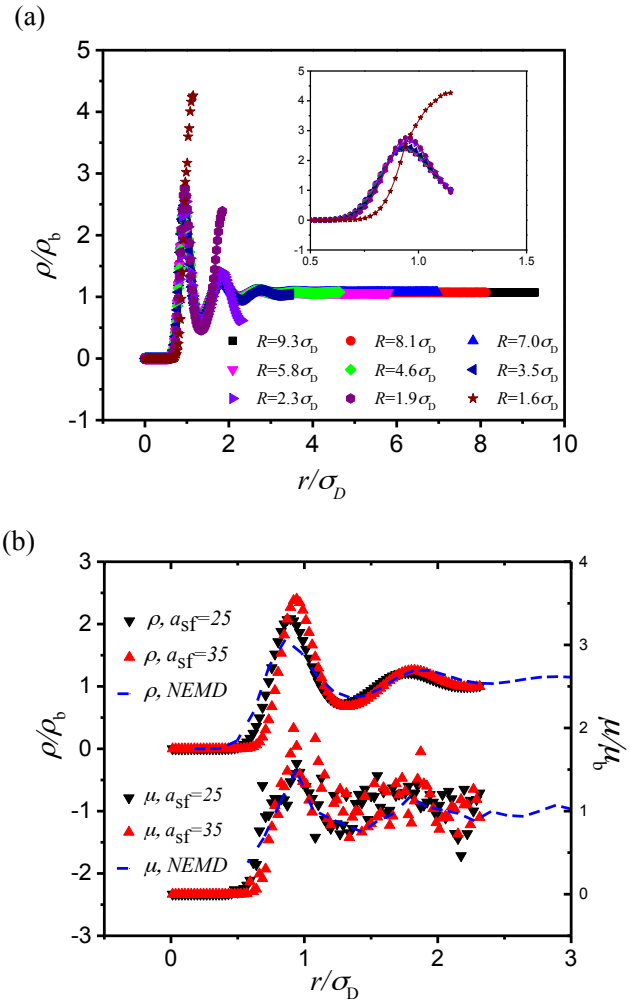

Fig. 1 (a) Density profiles with different radiuses. (b) Density and viscosity profiles with different wettability (NEMD: nonequilibrium molecular dynamics method).

The most important character we concern about the nanotubes in almost all the applications is the penetration rate, namely the flux per unit driving force. The flow enhancement ε is defined as the ratio of the simulated penetration rate to that

calculated by the Hagen-Poiseuille relation with the average density and viscosity of the system:

$$\varepsilon = \frac{Q_{\text{sim}}}{Q_{\text{pois}}} \tag{1}$$

As shown in **Fig. 2**, the enhancement increases with the decrease of the radius and the wettability and can exceed hundreds in some cases. The previous work by Thomas *et. al.*[15] with molecular dynamics simulation has revealed similar tendency, which is also displayed in **Fig.2**. The quantitative difference lies in the different force fields and wettability while the results share the same magnitude. The theoretical analysis in their paper[15] accounted for the inaccurate prediction with the inhomogeneous region and proposed a revised expression with the radius-dependent slip length and the radius-dependent viscosity which represents a cross-sectional averaged effective viscosity of the viscosity at a specific position in the inhomogeneous region and that of the bulk region. When we apply it with the data in this work, an underestimate is found as shown in **Fig.2**. For the drastic inhomogeneity, it is difficult to abstract a representative viscosity in the inhomogeneous region and it badly affects the precision of calculation. Therefore, a full consideration of the property variance is a more reliable replacement.

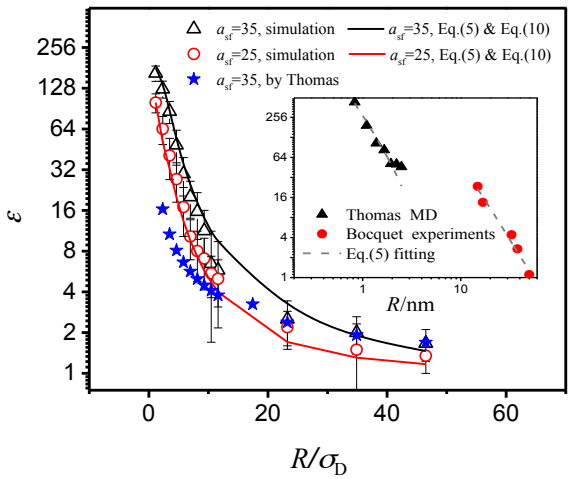

Fig. 2 Comparison between theoretical and simulated flow enhancement. The spots with error bars are the DPD simulation results. The corresponding lines are the theoretical results with the method proposed in this work. Eq.10 is applied to the cases with $R<3\sigma_D$, and Eq.5 is applied to those with $R>3\sigma_D$. The stars denote the calculation with the method proposed by Ref.12 with our data. The inserted image shows the fitting of previous reported enhancement by the model we proposed.

3 Theoretical Analysis

The enhancement stems from the distortion of the velocity profile caused by the inhomogeneity. Starts with the Stokes equation as many classical theories, when the fluid inhomogeneity is taken into consideration and the flow is driven by the body force, we have

$$\frac{1}{r}\frac{\mathrm{d}}{\mathrm{d}r}\left(r\mu(r)\frac{\mathrm{d}v_x}{\mathrm{d}r}\right) = -\rho(r)f_x \tag{2}$$

where r is the radial position; v_x is the axial velocity; ρ and μ respectively denote to the density and the viscosity. f_x is the body force applied to the fluid particles. With the assumption that the fluid velocity on the solid boundary is zero, one can have the velocity distribution in both the inhomogeneous and bulk regions as

$$v_x^{\text{i}}(r) = \left[v_s + \int_{R-\delta}^{R}\frac{\int_r^R r'\rho(r')f_x\,\mathrm{d}r'}{r\mu(r)}\mathrm{d}r\right]\left[\frac{\int_r^R \frac{\mathrm{d}r}{r\mu(r)}}{\int_{R-\delta}^{R}\frac{\mathrm{d}r}{r\mu(r)}}\right] - \int_r^R \frac{\int_r^R r'\rho(r')f_x\,\mathrm{d}r'}{r\mu(r)}\mathrm{d}r \tag{3}$$

$$v_x^{\text{b}}(r) = v_s + \frac{\rho_b f_x}{4\mu_b}\left[(R-\delta)^2 - r^2\right] \tag{4}$$

Where R is the radius of the nanotube; μ_b and ρ_b refer to the bulk viscosity and density, and v_s is the velocity at the two regions interface that can be determined by the matching of velocity and the shear stress. δ is the thickness of inhomogeneous region. With the velocity expressions Eqs. (3) and (4) for the inhomogeneous and bulk regions, one can obtain the penetration rate with the contribution of both regions as

$$\begin{aligned}\frac{Q}{f_x} &= \frac{1}{\pi R^2}\left[\int_{R-\delta}^{R}\rho(r)v_x^{\text{i}}(r)\cdot 2\pi r\,\mathrm{d}r + \int_0^{R-\delta}\rho v_x^{\text{o}}(r)\cdot 2\pi r\,\mathrm{d}r\right]\\ &= \frac{\rho_b^2 R^2}{\mu_b}\left[\left(\frac{\delta}{R}\right)^4\left(\frac{A_1}{2R}+\frac{1}{8}\right)+\left(\frac{\delta}{R}\right)^3\left(-\frac{3A_1}{2R}+\frac{1}{2}\right)-\left(\frac{\delta}{R}\right)^2\left(-\frac{3A_1}{2R}+\frac{3}{4}\right)\right.\\ &\quad\left.+\left(\frac{\delta}{R}\right)\left(\frac{A_1}{2R}-\frac{A_2}{R^2}-\frac{1}{2}\right)+\left(\frac{A_2}{R^2}+\frac{2A_3}{R^3}+\frac{1}{8}\right)\right]\end{aligned} \tag{5}$$

where

$$\begin{aligned}A_1 &= \int_{R-\delta}^{R}\frac{R\mu_b}{r\mu(r)}\mathrm{d}r\\ A_2 &= \int_{R-\delta}^{R}\frac{R\mu_b\int_{R-\delta}^{r}\frac{r'\rho(r')}{R\rho_b}\mathrm{d}r'}{r\mu(r)}\mathrm{d}r\\ A_3 &= \int_{R-\delta}^{R}\frac{r\rho(r)}{R\rho_b}\left[\int_r^R\frac{R\mu_b\int_{R-\delta}^{r'}\frac{r''\rho(r'')}{\rho_b}\mathrm{d}r''}{r'\mu(r')}\mathrm{d}r'\right]\mathrm{d}r\end{aligned} \tag{6}$$

The parameters A_1, A_2 and A_3 are of O(δ), O(δ^2) and O(δ^3) respectively. Different from the nanoslit in which we have proved the independence between these parameters and the slit size and all the parameters are exclusively determined by the wettability[20], A_1, A_2 and A_3 are radius-dependent in nanotubes because of the curvature. As the density/viscosity distributions

are still independent of tube size, R here can only exert influences on these three parameters when it is comparable to δ. When R gets larger, however, the parameters become stable. Then we studied the tendency of A_1/R, A_2/R^2 and A_3/R^3 while enlarging R. Fig. 3 demonstrates that firstly those three terms are with similar magnitudes, and then they all shrink rapidly as R increases and approach to zero in the end. Therefore, we can gradually eliminate the terms of higher order traces to achieve simplification for the less confined tubes. For instance, when the terms with (δ/R), $(\delta/R)^2$ and $(\delta/R)^3$ are neglected, the expression of penetration rate can be simplified to

$$\frac{Q}{f_x} = \frac{\rho_b^2 R^2}{\mu_b}\left[\frac{1}{8} + \frac{A_2}{R^2} + \frac{2A_3}{R^3}\right] \quad (7)$$

Eq.(7) resembles the Navier's equation which introduces the effective slip length λ_e into the Hagen-Poiseuille relation as

$$\frac{Q}{f_x} = \frac{\rho_b^2 R^2}{8\mu_b}\left[1 + \frac{\lambda_e}{4R}\right] \quad (8)$$

Eq.(8) is based on the Navier's condition[22], involving the hydrodynamic slip with the parabolic velocity pattern persisting. So in the use of this equation, the actual velocity profile is substituted by an approximate parabola coming from the extension of the bulk velocity profile. When R becomes furtherly enlarged, the terms with (A_2/R^2) and (A_3/R^3) in Eq.(7) are similarly ignored, an ultimate simplification leads to the Hagen-Poiseuille relation:

$$\frac{Q}{f_x} = \frac{\rho_b^2 R^2}{8\mu_b} \quad (9)$$

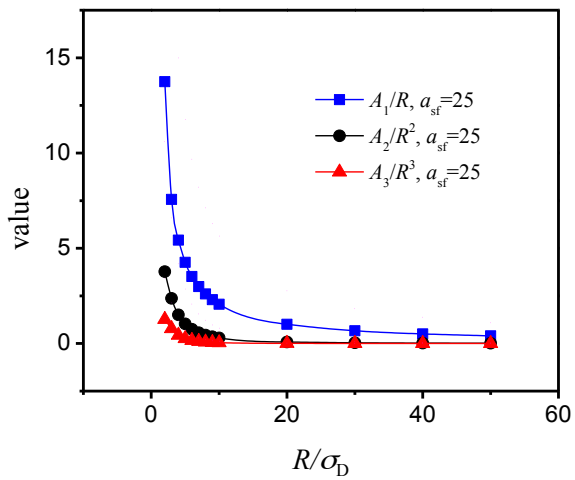

Fig. 3 Variation of the value of A_1/R, A_2/R^2 and A_3/R^3 with radius.

In another situation when the tube radius is extremely small and the inhomogeneous region from different directions overlaps, the plug-like flow is observed (**Fig. S4**). In such flow, velocity is approximately uniform regardless of position, and is proportional to the driving force:

$$f_x = cv_x \quad (10)$$

where c is the friction coefficient which can be obtained by testing simulations. Some previous works demonstrated that in such extremely narrow channels, the fluid may assemble in specific structures[23,24] when the DPD method is not suitable and a more detailed simulation method is required.

The inhomogeneous model and its simplified editions, together with the friction model can provide a general usability in tubes ranging from nano to bulk scales. We provide the calculated results with the models in Fig. 2 and it is in good agreement with the penetration rate by simulation. To be specific, Eq.(5) is used for the tubes with $R>3\sigma_D$ and Eq.(10) for those with $R<3\sigma_D$. We need to remark that the inhomogeneous distributions of density and viscosity used in the calculations are all extracted from the cases with $R=9.3\sigma_D$ and they work well to predict the parameters with different R but the same wettability. Thus we applied Eq.(5) to the reported results of flow enhancement[8,13] and good agreement can be found in **Fig. 2.**

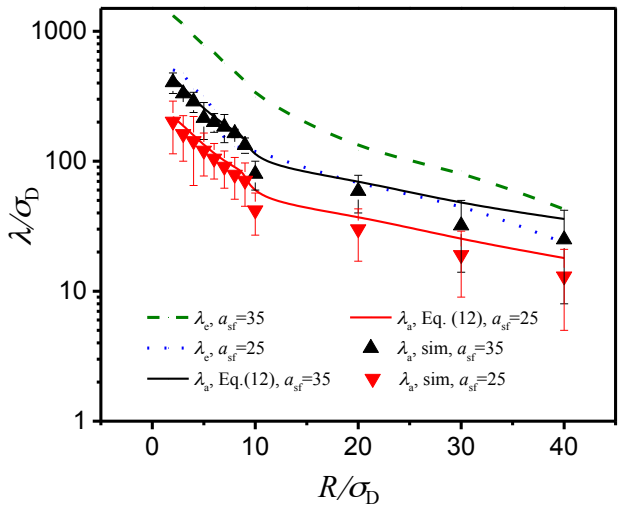

Fig. 4 Comparison between theoretical and simulated apparent slip lengths within wettable and non-wettable nanotubes.

When the enhancement is attributed to a surface slippage alone as Eq.(8), the slip length is called the effective slip length λ_e and it is always reported in experimental works. We calculate

the effective slip length with the enhancement results and display it in Fig. 4. However there is another concept of slippage, the apparent slip λ_a, which is defined by the Navier's condition[22] as

$$v_x^b(R) - v_{wall} = -\lambda_a \left. \frac{dv_x^b}{dr} \right|_{r=R} \quad (11)$$

where v_{wall} is the fluid velocity at the solid/liquid interface and we assume it to be zero in this case. With Eq.(4) we have the apparent slip expressed with the previous parameters as

$$\lambda_a = A_1 \frac{(R-\delta)\delta}{R^2} + \frac{2}{R} A_2 + \frac{\delta^2}{2R} - \delta \quad (12)$$

The details of the derivation process for both the penetration rate and the slip length are displayed in the SI, section 4. **Fig. 4** demonstrates good agreement between the calculated apparent slip lengths and those observed from the velocity profiles in simulation. It is found that both the apparent slip length and the effective ones are negatively related to the tube radius, and ultimately approximate zero as the general recognition of no-slip condition in bulk scale. Such tendency is coincident with Bocquet's finding from experiment[8]. In addition, we also find the slip length increases with the increase of hydrophobicity in both the cases. However, the gap between the effective and apparent slip lengths especially in narrow tubes cannot be ignored. As the effective slip is deduced from the enhancement results and the apparent slip is obtained from the bulk velocity profiles, the gap just clarifies that the bulk velocity profile cannot extend to the surface and there is a region with inhomogeneity aside the walls.

To clarify the DPD unit in this work, an order of magnitude analysis is conducted according to the scaling method used by Groot[25]. As a result the length and time unit of a DPD simulation can find their corresponding real scale as

$$r_C \approx 5 \times 10^{-10} [\mathrm{m}] \quad (13)$$

$$\tau \approx 6 \times 10^{-11} [\mathrm{s}] \quad (14)$$

Therefore the velocity scale is

$$(\quad r_C / \tau \approx 10 [\mathrm{m \cdot s^{-1}}] \quad 15)$$

Thus the order of magnitude of the velocity results in this work is about 1×10^{-1} m/s, which is much closer to the experimental results[1] than the MD simulations[26]. The efficiency of DPD can be found from the scaling, as the time scale in this case can easily be above microsecond and the length scale can also reach micrometer. We estimate the Reynolds number to be of 1×10^{-4} in strongly confined tubes and 1×10^{-3} in larger tubes. Which is definitely small and that's why the Stokes Equation (Eq.2) can be used as the starting point of the deviation.

In previous reports, the contact angle of water and carbon nanotubes are at 90 degree or more than 100 degree[27,28]. As shown in Fig. S2, the a_{sf} we choose as 25 and 35 respectively denote the contact angles of 90° and 120°. So the cases can be matched with the water-carbon nanotube system. The effective slip length in this work, when transformed into real scale, turns out to be 10.8-626.0 nm, which is close to the experimental results (10-1000nm) reported in previous works[26]. The apparent slip lengths, however, are relatively small at about 8.5-208.0 nm.

4 Conclusion

To conclude, with the DPD simulation, we observe the inhomogeneity of the local density and viscosity, whose independence with the tube size provides great convenience for theoretical works. By introducing the density and viscosity inhomogeneity into the Stokes equation, we derive the counterpart for the Hagen-Poiseuille relation in nano-confined systems, which is validated by DPD simulation. It is intriguing but reasonable that the proposed model for penetration rate can be simplified into the Hagen-Poiseuille relation when the spatial confinement can be ignored, which makes it valid throughout all scales and significant to explain the evolutionary process for fluid flow from nano to bulk scales. When applied to existing experimental data, the model shows great applicability. And then we derive a theoretical expression for apparent slip length, which is inversely related to tube size. We find the effective slip length is larger than the apparent slip length which implies the fluid inhomogeneity plays a part to enhance the flow.

The possible directions on which we can take use of the models are twofold. One relies on more accurate calculation which may be in a theoretical way rather than numerical ways. For instance, the density-functional theory may be helpful to obtain the local density with a given solid surface, and the viscosity can be therefore estimated as some works have already revealed its positive relation with the local density[11]. Together with the model we proposed, precise calculation can be achieved in the future. The other way seems more foreseeable, especially in those less-confined tubes where the flow rate can be measured. As the local density/viscosity are independent of the tube size and the curvature is negligible in those tubes, the 3 parameters in Eqs.5 for a particular material can be summarized from the fitting of 5 or more points with different pore sizes. In addition, with the method introduced in this work and the help of the electrical double-layered theory, the model can be extended to the nano-confined flow driven by different forces, including electric fields, pressure drops and chemical gradients.

As for the extremely narrow tubes (which we mentioned as the tubes with overlapped inhomogeneous regions), the friction model can be a direction. However, how to correlate the friction coefficient with the macroscopic properties of the tube is a problem. In this case, we are facing with not only the break-down of continuous equations but also the unreliable of classic force field in discrete simulations. The ab initio molecular dynamics simulation may be a choice, but we also realize that the gap of time- and length-scale

between the ab initio molecular dynamics and the reality is even more enormous.

Acknowledgements

Financial supports from the National Natural Science Foundation of China (21490584, 91534105), National Key Research and Development Program (2016YFB0301701), Major National Scientific Instrument Development Project (21427814) and Jiangsu National Synergetic Innovation Center for Advanced Materials are gratefully acknowledged.

Notes and references

1. M. Majumder, N. Chopra, R. Andrews, B. J. Hinds, *Nature,* **2005,** *438*, 44.
2. J. R. Werber, C. O. Osuji, M. Elimelech, *Nature Reviews Materials,* **2016**,1,16018.
3. L. Li, J. Mo, Z. Li, *Phys. Rev. Lett.,* **2015,** *115*, 134503.
4. F. Fornasiero, H. G. Park, J. K. Holt, M. Stadermann, C. P. Grigoropoulos, A. Noy, O. Bakajin, *Proc. Natl. Acad. Sci. USA,* **2008,** *105* (45), 17250-5.
5. B. Corry, *J. Phys. Chem. B,* **2008,** *112*, 1427-1434.
6. A. Alexiadis, S. Kassinos, *Chem. Rev.* **2008,** *108*, 5014–5034.
7. E. Lauga, M. P. Brenner, H. A. Stone, *Handbook of Experimental Fluid Mechanics*. Springer: New York, 2007.
8. E. Secchi, S. Marbach, A. Niguès, D. Stein, D.; A. Siria, L. Bocquet, *Nature* **2016,** *537*, 210-213.
9. D. Mattia, F. Calabro, *Microfluid Nanofluid*, **2012**,13,125–130
10. K. Falk, F. Sedlmeier, L. Joly. R. R. Netz, L. Bocquet, *Nano Lett.* **2010,** *10*, 4067–4073.
11. H. Hoang, G. Galliero, *Phys. Rev. E* **2012,** *86*, 021202.
12. Hoang, H.; Galliero, G. Shear viscosity of inhomogeneous fluids. *J. Chem. Phys.* **2012,** *136* (12), 27-31.
13. S. Pronk, E. Lindahl, P.M.Kasson, *Nature Commun,* **2014,** *5*(1), 155-164.
14. T. Mayers, *Microfluid. Nanofluid.* ,**2010,** *10*(5), 1141-1145.
15. J.A.Thomas, A.J.H.McGaughey, *Nano Lett.,* **2008,** *8* (9), 2788-2793.
16. D.Mattia, F.Calabro, *Microfluid. Nanofluid.,* **2012,** *13*, 125-130.
17. M.Ma, F. Grey, L. Shen, M.Urbakh, S. Wu, J.Z Liu, Y. Liu, Q.Zheng, *Nature Nanotechnology,* **2015,** *10*, 692-696.
18. T.A.Pascal, W.A Goddarda, Y.Jung, *Proc. Natl. Acad. Sci. USA,* **2011,** *108* (29), 11794–11798.
19. M.Whitby, L.Cagnon, M.Thanou, N.Quirke, *Nano Lett.,* **2008,** *8* (9), 2632-2637.
20. Y.Y.Wang, J.B.Xu, C.Yang, AIChE J.2017,63(2):834-842.
21. J.H.Irving, J.G. Kirkwood, *J. Chem. Phys.,* **1950,** *18*, 817.
22. C.L.M.H.Navier, *Mem. Acad. Sci. Inst. Fr.,* **1823,** *1*, 414.
23. J.A.Thomas, A.J.H.McGaughey, *Phys. Rev. Lett.* **2009,** *102*, 184502.
24. A. Striolo, *Nano Lett*., **2006**, 6 (4), 633-639.
25. R.D.Groot, *Langmuir* **2000,** *16*(19), 7493-7502.
26. S.K.Kannam, B.D.Todd, J.S.Hansen, P.J.Daivis, *J. Chem. Phys.* **2013,** *138*, 094701.
27. A.W.Adamson, A.P.Gast, Physical Chemistry of Surfaces, 6th Edition, Wiley: New York, **1997**.
28. T. Werder, J. H. Walther, P. Koumoutsakos, *Nanotechnol.*, **2002,** *50*, 29-55.